Performance Characteristics of a Direct Ammonia Fuel Cell with an Anion Exchange Membrane

Yun Liu[a], Zhefei Pan[a], Oladapo Christopher Esan[a], Liang An[a,*]

[a] Department of Mechanical Engineering, The Hong Kong Polytechnic University, Hung Hom, Kowloon, Hong Kong SAR, China

*Corresponding author.

Email: liang.an@polyu.edu.hk (L. An)

Abstract

In this work, a direct ammonia fuel cell, which composes of an anion exchange membrane and the commercially available PtRu/C and Pd/C catalysts at the anode and cathode, respectively, is developed. Experimental results demonstrate that the direct ammonia fuel cell exhibits a peak power density of 20.7 mW cm^{-2} and an open-circuit voltage of 0.67 V at 95 ℃ when running on the fuel solution using 3.0 M ammonia and 3.0 M KOH. In addition, the effects of operating parameters, such as the concentrations of ammonia and KOH, flow rates of anolyte and oxygen, and operating temperatures on the cell performance are experimentally examined. Higher KOH concentration is observed to increase the cell voltage by enhancing the kinetics of ammonia oxidation, which is facilitated by the higher concentration of OH^- in the catalyst layer. However, increasing the KOH concentration leads to higher internal resistance in the cell due to the increased viscosity of the anolyte. Besides, the analysis of results suggests that a moderate flow rate of both anolyte and gas can also enhance the cell performance by reducing ammonia crossover and preventing membrane dehydration, respectively. Moreover, increasing the operating temperature of the cell also promotes the kinetics

of the electrochemical reactions at the catalyst layer which is also associated with an enhanced mass transfer within the electrode. In summary, a direct ammonia fuel cell, using an anion exchange membrane, with relatively high performance has been developed, and the study provides insights into the performance-enhancing strategies via operating conditions towards its further development.

Keywords: Ammonia, direct ammonia fuel cells, anion exchange membrane, operating parameters, power density

1. Introduction

Proton exchange membrane fuel cells (PEMFC) have been considered as one of the most promising electricity generation techniques, due to their high efficiency and zero-emission [1,2]. However, hydrogen, as the lightest gas, is difficult to be compressed (~70 MPa) and liquefied (-252.9 ℃) [3]. As a result, the handling, storage, and transportation of hydrogen are challenging and costly, which hinders the implementation and commercialization of PEMFC [4–7].To address this issue, it becomes necessary to explore fuels that are easy to store and transport. Therefore, the liquid fuels, including those that are liquid or easy to liquefy at ambient conditions, have received extensive attention from researchers [8–11]. In recent years, alcohol-based fuels such as methanol and ethanol have been widely used in fuel cells due to their ease of storage and transportation [12]. Nevertheless, the application of alcohols in fuel cells still emits carbon dioxide and requires additional carbon capture technology to achieve zero emissions [13].

By contrast, ammonia (NH_3), which can be liquefied under mild conditions, is a carbon-free fuel with a hydrogen content as high as 17.65% [14]. More importantly, ammonia-ready storage and transportation infrastructure can promote the safe, cheap and efficient shipping of ammonia [15–17]. These advantages thus positioned ammonia as an ideal fuel for energizing fuel cells [18–21]. The first ammonia fuel cell was developed in the 1960s by Cairns and Simons through using KOH as the electrolyte, which greatly promotes the research and development of ammonia fuel cells [22]. Over the past few

decades, direct ammonia fuel cells (DAFCs), have received ever-increasing attention among researchers [23] and significant progress has thus been achieved [24]. For instance, Silva et al. developed a DAFC consisting of a Nafion 117 membrane, PtAu/C catalyst at the anode, and Pt/C catalyst at the cathode. An open-circuit voltage (OCV) of 0.588 V and a peak power density of 2.64 mW cm^{-2} were achieved [25]. In another study conducted by Assumpcao et al., a relatively higher power density of 5.37 mW cm^{-2} was realized by a DAFC that employed the same proton exchange membrane (Nafion 117), PtRh/C catalyst at the anode, and Pt/C catalyst at the cathode [26]. In addition to the achieved progress in exploring the advanced catalyst material, the electrolyte material has also been investigated. Suzuki et al. [17] applied a different type of membrane, i.e., the anion exchange membrane (AEM), as the solid electrolyte for the operation of DAFCs. Their results showed that a peak power density of 3.07 mW cm^{-2} was realized by employing an AEM. Despite the progress made in the last few decades, the power output of DAFCs is still apparently low, below 10.0 mW cm^{-2} [27–29]. Interestingly, a breakthrough was achieved in 2019 by a research group led by Professor Yan at The University of Delaware, which developed an advanced membrane and demonstrated the potential of DAFCs for future practical applications [30].

In addition to the application of DAFC, ammonia can be indirectly used in fuel cells by cracking into hydrogen. Recently, an ammonia-powered fuel cell electric vehicle has been developed and manufactured by a research group led by Professor Eric Cheng and Professor Molly Li at The Hong Kong Polytechnic University [31]. Besides producing

zero carbon emissions, the vehicle would also be more efficient and provide safer storage of energy than conventional electric vehicles.

Although promising, the DAFC performance must be substantially improved before widespread application becomes possible [32,33]. The realization of performance improvement depends not only on the development of novel electrocatalytic and membrane materials, but also on the innovation and optimization in the electrode-level and cell-level designs, which requires the critical understanding of two-phase flow, mass/charge transport and electrochemical reactions simultaneously occurring in this multi-scale and multi-layer cell.

In summary, the previous studies have predominantly been focused on the development of materials such as catalysts and membranes. However, the mass/charge transport at the cell level, which has a great impact on the cell performance, has not been thoroughly studied. Therefore, relevant research should be conducted to provide insight into DAFCs from a fundamental perspective. In this work, a DAFC with an AEM and the commercial PtRu/C and Pd/C electrocatalysts at the anode and cathode, respectively, are developed. In addition, the effects of various operating parameters, including the concentrations of ammonia and KOH, flow rates of anolyte and oxidant, and the operating temperature on the DAFC performance are experimentally examined.

2. Working Principle

Fig. 1a illustrates the working principle of a DAFC, which composes of a membrane electrode assembly (MEA) for the electrochemical reactions to occur, and a flow field

for supplying reactants and removing products. The MEA is composed of an AEM, an anode catalyst layer (ACL) and an anode diffusion layer (ADL), a cathode catalyst layer (CCL), and a cathode diffusion layer (CDL). To provide a more comprehensive understanding of the DAFC, both the physical and chemical processes which simultaneously occur in a DAFC are presented in Fig. 1. At the anode, the ammonium hydroxide is fed into the cell using a pump and flows through the flow channel, passes through the interface between the flow channel and diffusion layer, and then diffuses into the diffusion layer. At the diffusion layer, due to the concentration gradients of ammonia and the existence of pressure differences in the adjacent flow channels, the mass transport behavior of ammonia includes diffusion and convection. The ammonia thereafter moves from the ADL to the ACL due to the driving force caused by the difference in ammonia concentration. The ammonia then reacts with OH^- and produces nitrogen and water, and releases electrons according to Eq. 1 [34]:

$$2NH_3 \cdot H_2O + 6OH^- \rightarrow N_2 + 8H_2O + 6e^-, \qquad E_a^0 = -0.77 \text{ V vs. SHE} \tag{1}$$

The produced electrons at the anode, which are driven by the electric potential difference between anode and cathode, transfer through the external circuit and arrive at the cathode, creating an electric current. At the CCL, water and oxygen react with electrons to produce OH^- according to Eq. 2 [35]:

$$\frac{3}{2}O_2 + 3H_2O + 6e^- \rightarrow 6OH^-; \qquad E_c^0 = +0.40 \text{ V vs. SHE} \tag{2}$$

Meanwhile, due to the electric field that existed between two electrodes, the OH^- generated at the CCL will migrate through the AEM to the anode catalyst layer to generate the ionic current. Thus, the overall electrochemical reaction equation of the DAFC can be obtained as Eq. 3:

$$2NH_3 \cdot H_2O + \frac{3}{2}O_2 \rightarrow N_2 + 5H_2O; \qquad E^0 = 1.17 \text{ V} \tag{3}$$

Based on Eq. 3, the theoretical voltage of this DAFC is 1.17 V. However, the measured voltage from the experiments is much lower at around 0.6 V. This could be generally attributed to the performance degradation in fuel cells during their real operations caused by electrochemical polarization, ohmic polarization, and concentration polarization [36,37]. Meanwhile, there is a tendency that the ammonia in the ACL would transport through the membrane and arrive at the CCL because the ammonia concentration on both sides of the membrane is different and the membrane is permeable to ammonia. This phenomenon, also known as ammonia crossover, results in loss of fuel. Meanwhile, the ammonia that arrived at the cathode will be oxidized to form a mixed potential that further reduces the voltage of the fuel cell [38].

3. Experimental section

3.1 Preparation of an MEA

The MEA, consisting of an anode, a membrane, and a cathode with an active area of 1.0 × 1.0 cm^2, is prepared first. The anode is a commercially available electrode obtained from Johnson Matthey, USA, the anode catalyst is composed of PtRu/C (1:1 atom%) with total PtRu loading of 4.5 mg cm^{-2}. The selection of PtRu/C as an anode ammonia oxidation catalyst for this research work included following considerations: (1) According to Chen et al, direct ammonia fuel cells with PtRu/C as catalyst exhibit higher open circuit voltages as well as peak power densities when using PtRu/C versus Pt/C as the anode catalyst for direct ammonia fuel cells [39]. (2) Kormanyos et al. [40] investigated the effect of ammonia on the stability of PtRu/C in acidic and alkaline media. Their results show that PtRu/C can maintain good stability in the operation of ammonia-based fuel cells. The cathode is a homemade electrode with a commercially

available catalyst (Pd/C). The main reason for choosing Pd was because of the problem of ammonia poisoning of the cathode catalyst. During the experiments, the ammonia from the anode would diffuse across the membrane to the cathode catalyst layer and then be oxidized. If conventional Pt is used as the cathode catalyst, the intermediate product of ammonia oxidation, N*, will lead to the toxic deactivation of the cathode catalyst Pt, thus affecting the performance of the ammonia fuel cell [41] In contrast, according to previous studies, Pd is insensitive to the adsorbed N produced during ammonia oxidation and has some resistance to poisoning [42] Following these considerations, Pd was chosen as the cathode catalyst. The electrode fabrication process of the Pd/C is illustrated as follows: (1) Preparation of catalyst ink. The catalyst ink is obtained by mixing the Pd/C powder (10.0 wt. %, Sigma-Aldrich Co., USA) with ethanol (99.9 wt. %. as the solvent), and Nafion (5.0 wt. %, as the binder). As shown in Fig. 1, the water will transport from ACL to CCL due to the membrane is permeable to water as well as the water gradient next to the membrane. Water will fill the free volume within the Nafion binder on the CCL, which can then transport OH^- driven by the existing electric field [43]. An ultrasonic stirring process is then used to mix the solution uniformly. (2) Spraying the catalyst ink onto the surface of carbon paper (Toray TGP-H-090, 280 μm) with a spray gun. Afterward, a dual-layer electrode (i.e. catalyst layer and diffusion layer) is obtained. In this work, the cathode catalyst loading is around 0.55 mg cm^{-2}. The membrane applied in this work is an AEM with OH^- as the charge carrier in DAFCs. Fumasep FAS-30 (Fuel Cell Store, USA), with a rough thickness of 30 μm, was applied as the AEM. The procedure for the AEM pretreatment is as follows: (1) immerse the membranes into a prepared 1.0 M KOH solution for 24.0 hours, (2) wash the modified membrane with deionized water to remove any contaminants.

3.2 Experimental setup

To fix the MEA, two plates are applied for anode and cathode at the outer side as support (see Fig. 1b). Additionally, two gaskets are used to prevent any form of leakage from the MEA. The flow field applied in this study is a single serpentine flow channel slotted by wire cutting technology with a depth and width of 1.0 mm and 0.5 mm, respectively. The reactants are fed into the cell by using the peristaltic pump. The anolyte is prepared by mixing ammonia and KOH using different concentrations. The flow rate of the anolyte is regulated by a peristaltic pump, ranging from 2.0 to 6.0 mL min^{-1}. Pure oxygen is used as the oxidant at the cathode with a gas flow rate increasing from 10 to 100 standard cubic centimeters per minute (SCCM). In this work, the anode solution was indirectly heated by heating the fuel cell device using an additional heating device (heat rod) and the temperature is measured by thermocouples. The DAFC performance test is conducted by an Arbin BT2000 (Arbin Instrument Inc.).

4. Results and discussion

4.1 General performance

The performance test results of the developed DAFC are presented in Fig. 2, using an anolyte containing 3.0 M ammonia in 3.0 M KOH with a flow rate of 2.0 mL min^{-1} at 95 ℃, and pure oxygen feeding into the cell as the oxidant with a flow rate of 10 SCCM. The results show that the maximum current density is around 150.0 mA cm^{-2}. An OCV of 0.67 V with a peak power density of 20.7 mW cm^{-2} are achieved. The improved performance of this DAFC can be explained by the enhanced kinetics of ammonia oxidation at the anode catalyst layer due to the high concentrations of OH^- and the relatively high operating temperature (95 ℃) [44]. Another important factor that contributes to the improved cell performance is the low internal resistance due to the application of a thinner membrane, with its thickness around 30 μm.

4.2 Effect of the KOH concentration

The effect of OH^- concentration on the developed DAFC performance was examined by using different concentrations of KOH solution increased from 1.0 to 9.0 M. During the test, the ammonia concentration was maintained at 3.0 M. The anolyte flow rate was set at 2.0 mL min^{-1} and the oxygen flow rate was set at 10 SCCM. The operating temperature was set at 95 ℃. As shown in Fig. 3, results reveal that the voltage of the DAFC increases with increasing KOH concentrations. The reason is that a higher concentration of KOH fed into the flow field will lead to a high OH^- concentration gradient from the bulk flow to the interface between the anode flow field and the ADL, and then from the ADL to the ACL. As a result, the OH^- concentrations in the anode catalyst layer will increase due to the enhanced diffusion caused by the higher OH^- concentration gradient. According to Eq. 1, it can be inferred that higher OH^-

concentrations will improve the kinetics of ammonia oxidation [45]. More specially, the absorption of OH^- to the surface of the catalyst would be much easier compared to a low concentration of OH^-. Hence, the ammonia oxidation efficiency will be improved. However, as the OH^- concentration increased from 1.0 M to 9.0 M, the measured resistance value of the fuel cell gradually increases from 600 mΩ to 1132 mΩ. This could be attributed to the increase of the electrolyte viscosity as the concentration of KOH increases. In this way, the mass transport processes in the anode, such as reactant adsorption and product desorption on the catalytic layer of the anode, are slowed down such as the diffusion process of ammonia and OH^-. In other words, the resistance to mass transfer in the fuel cell increases, thus making the overall resistance of the fuel cell increase thereby leading to a larger ohmic loss [46]. Following this, it can be concluded that the increase of alkali concentration will lower the DAFC performance. Interestingly, the results presented in Fig. 3 reveal that the highest peak power density is obtained at the KOH concentration of 3.0 M. The behavior can be explained by the tradeoff between the positive effects of improved voltage and the negative effects of increased ohmic loss associated with higher KOH concentrations.

4.3 Effect of the ammonia concentration

In addition to examining the effect of KOH concentration, it is also necessary to determine the effect of ammonia concentration on the DAFC performance. Here, the KOH concentration was maintained at 3.0 M while ammonia concentration was tested at 1.0, 3.0, and 5.0 M. Experimental results demonstrated in Fig. 4 show that the increment of ammonia concentration from 1.0 M to 3.0 M will improve both the OCV and peak power density of the DAFC. It can be explained by the increased concentration of ammonia in the ACL, caused by gradient enlargement from the flow field to the ACL, resulting in enhanced fuel diffusion [47]. However, further increasing the ammonia concentration from 3.0 to 5.0 M resulted in performance degradation of the fuel cell. As the applied AEM is permeable to ammonia, the ammonia crossover is easy to occur when the ammonia concentration in the catalyst layer on the anode is high. Afterward, the ammonia arrived at the catalyst layer on the cathode will be oxidized by the Pd catalyst. This oxidation process also releases electrons and therefore an inner electrons flow will be formed in the CCL, producing a mixed potential in the cathode and lowing the cell performance. In summary, the high performance of DAFC can be achieved with a moderate anolyte flow rate.

4.4 Effect of the oxygen flow rate

The effects of various gas flow rates on the DAFC performance were tested. The obtained results shown in Fig. 5 indicate that the performance of the DAFC decreases with the increment of oxygen flow rates. The reason could be summarized as follows: the oxygen used in this study is directly fed into the cathode flow field without humidification. Consequently, the water molecules on the cathode catalytic layer are

quickly swept out of the cathode by the oxygen flow. If the gas flow rate is too large, the water molecules in the membrane near the cathode side will also be blown away, resulting in a decrease in the water content and eventually dehydration of the membrane. In addition, the AEM is more susceptible to dehydration at high operating temperatures [48]. As a result, the conductivity of the membrane is severely reduced, thereby leading to an increase in the internal resistance of the cell. The measured value of the internal resistance of the DAFC under various gas flow rates reveals that DAFC resistance increased by approximately 500 mΩ as the gas flow rate was increased from 10 to 100 SCCM, thereby reducing the performance of the cell. Therefore, when the pure oxygen is directly applied as an oxidant without humidification, a relatively low gas flow rate would be an ideal choice to improve the cell performance.

4.5 Effect of the anolyte flow rate

The effects of various flow rates of the anolyte on the DAFC performance were also studied. The results as summarized in Fig. 6 show that the performance of the DAFC decreases with the increment of the anolyte flow rate. The main reason is that ammonia crossover is prone to occur at high anolyte flow rates [49]. More specially, because the ammonia is only supplied to the anode, the concentration of ammonia on the ACL is much higher than that of the CCL, resulting in a large ammonia concentration gradient difference on both sides of the membrane. Since the applied AEM allows the permeation of ammonia, the ammonia on the anode catalytic layer will pass through the membrane to the cathode catalyst layer. Then, the crossed ammonia will be oxidized to generate a mixed potential, thereby reducing the cell voltage. Meanwhile, the ammonia passivation of the anode catalyst PtRu/C and cathode catalyst Pd/C will be more severe as the concentration of ammonia is increased, thereby further reducing the cell performance. Based on the above analysis, it is suggested that a relatively low anolyte

flow rate should be applied to reduce the negative effects of ammonia crossover on the performance of DAFC.

4.6 Effect of the operating temperature

The operating temperature has a significant impact on the fuel cell performance [50]. In this section, the effect of operating temperatures on DAFC performance was examined. The experimental results shown in Fig. 7 demonstrate that increasing the temperature has significant impacts on improving the performance of DAFC. In particular, there is a performance leap when the operating temperature of the cell is increased from 80 to 95 ℃. It is found that the voltage and the peak power density of the developed cell gradually increase with increasing temperature, rising from 0.47 to 0.66 V and 1.70 to 19.68 mW cm^{-2}, respectively. This phenomenon can be explained by the following three reasons: firstly, the rising temperature will facilitate the kinetics of the oxygen reduction reaction (ORR) at the cathode and the ammonia oxidation reaction (AOR) at the anode, respectively [51]. As a result, the negative effects of activation loss on cell performance are reduced. Secondly, the rising temperature inside the fuel cell can accelerate the mass transport behavior of the electrode. In this case, the reactants are more easily transported to the active site, and the products are more easily transported backward from the CL through the DL to the flow field, thereby reducing concentration loss [52]. Thirdly, ion transport through the membrane will be accelerated when the operating temperature is increased. Hence, the membrane conductivity will increase, which will lead to a decrease in the internal resistance and a reduction in ohmic loss [53]. Our experimental findings validate that the internal resistance decreases from 1200 mΩ to around 650 mΩ as the temperature increases from room temperature to 95 °C. In summary, the operating temperature has a significant impact on DAFC

performance by affecting the kinetic of AOR and ORR, mass transport behavior, and membrane conductivity.

4.7 Constant-current discharging behavior

To verify the operation durability and stability of developed DAFC, a constant-current discharging test was performed using 3.0 ammonia in 3.0 M KOH as the fuel. The anolyte was circulated at a rate of 2.0 mL min^{-1} during the test, and the total volume of anolyte used was 200 ml. The pure oxygen was applied as the oxidant with a gas flow rate of 10 SCCM. The operating temperature was set at 95 ℃ and the current density of the discharging test was set at 20.0 mA cm^{-2}. The constant-current discharging curve of the DAFC was presented in Fig. 8, indicating that the assembled cell can maintain stable operation for more than 25 hours, and demonstrating the feasibility of applying an AEM to direct ammonia fuel cells. The overall performance degradation of the cell could be attributed to the ohmic loss and concentration loss during the operation. Another reason may be the catalyst poisoning and passivation due to the absorption of ammonia on the surface of PtRu and Pt nanoparticles surfaces, resulting in the degradation of catalyst activity, thereby affecting the durability of the developed cell.

5. Concluding remarks

In this work, a direct ammonia fuel cell, consisting of an anion exchange membrane, a PtRu/C electrocatalyst-based anode, and a Pd/C electrocatalyst-based cathode, is developed. Different experimental tests are afterward conducted to investigate the operation and performance of the DAFC. Performance tests reveal that the developed DAFC exhibits an OCV of 0.67 V and a peak power density of 20.7 mW cm^{-2} when operated using 3.0 M ammonia in 3.0 M KOH with an anolyte flow rate of 2.0 mL min^{-1} with pure oxygen as the oxidant with a gas flow rate of 10 SCCM. Furthermore, the effects of various operating parameters, such as the concentration of ammonia and KOH, flow rates of anolyte and oxygen, and the operating temperature on the cell performance are experimentally examined. It has been observed that a higher KOH concentration increases the cell voltage by enhancing the kinetics of ammonia oxidation in the catalyst layer, which is facilitated by the increased OH^- concentration. Increased concentrations of KOH, however, lead to higher internal resistance in the cell because of the increased viscosity of the anolyte. Besides, the analysis of the results also indicates that a moderate gas flow rate and anolyte flow rate are also effective in improving cell performance by preventing membrane dehydration and reducing ammonia crossover. Regarding the effect of the operating temperature, in addition to enhancing the kinetics of AOR and ORR at the anode and cathode catalyst layer, increasing the operating temperature of the cell also enhances the mass transfer between the electrodes. In summary, an anion exchange membrane DAFC with relatively high performance has

been developed, and the study provides insights into the performance-enhancing strategies via operating conditions towards the further development of DAFCs.

Acknowledgement

The work described in this paper was supported by a grant from the National Natural Science Foundation of China (No. 52022003) and a grant from the Shenzhen Science and Technology Innovation Commission (No. SGDX20201103095204 04).

References

[1] Y. Wang, B. Seo, B. Wang, N. Zamel, K. Jiao, X.C. Adroher, Fundamentals, materials, and machine learning of polymer electrolyte membrane fuel cell technology, Energy AI. 1 (2020) 100014. https://doi.org/10.1016/j.egyai.2020.100014.

[2] K. Jiao, J. Xuan, Q. Du, Z. Bao, B. Xie, B. Wang, Y. Zhao, L. Fan, H. Wang, Z. Hou, S. Huo, N.P. Brandon, Y. Yin, M.D. Guiver, Designing the next generation of proton-exchange membrane fuel cells, Nature. 595 (2021) 361–369. https://doi.org/10.1038/s41586-021-03482-7.

[3] M. Aziz, A. TriWijayanta, A.B.D. Nandiyanto, Ammonia as effective hydrogen storage: A review on production, storage and utilization, Energies. 13 (2020) 1–25. https://doi.org/10.3390/en13123062.

[4] C. Tarhan, M.A. Çil, A study on hydrogen, the clean energy of the future: Hydrogen storage methods, J. Energy Storage. 40 (2021) 102676. https://doi.org/10.1016/j.est.2021.102676.

[5] A.M. Elberry, J. Thakur, A. Santasalo-Aarnio, M. Larmi, Large-scale compressed hydrogen storage as part of renewable electricity storage systems, Int. J. Hydrogen Energy. 46 (2021) 15671–15690. https://doi.org/10.1016/j.ijhydene.2021.02.080.

[6] I.A. Hassan, H.S. Ramadan, M.A. Saleh, D. Hissel, Hydrogen storage technologies for stationary and mobile applications: Review, analysis and perspectives, Renew. Sustain. Energy Rev. 149 (2021) 111311.

https://doi.org/10.1016/j.rser.2021.111311.

[7] S. Liu, J. Liu, X. Liu, J. Shang, L. Xu, R. Yu, J. Shui, Hydrogen storage in incompletely etched multilayer Ti2CTx at room temperature, Nat. Nanotechnol. 16 (2021) 331–336. https://doi.org/10.1038/s41565-020-00818-8.

[8] M. Perčić, N. Vladimir, I. Jovanović, M. Koričan, Application of fuel cells with zero-carbon fuels in short-sea shipping, Appl. Energy. 309 (2022). https://doi.org/10.1016/j.apenergy.2021.118463.

[9] H.A. Elwan, M. Mamlouk, K. Scott, A review of proton exchange membranes based on protic ionic liquid/polymer blends for polymer electrolyte membrane fuel cells, J. Power Sources. 484 (2021) 229197. https://doi.org/10.1016/j.jpowsour.2020.229197.

[10] M. Hren, M. Božič, D. Fakin, K.S. Kleinschek, S. Gorgieva, Alkaline membrane fuel cells: Anion exchange membranes and fuels, Sustain. Energy Fuels. 5 (2021) 604–637. https://doi.org/10.1039/d0se01373k.

[11] N. Shaari, S.K. Kamarudin, R. Bahru, S.H. Osman, N.A.I. Md Ishak, Progress and challenges: Review for direct liquid fuel cell, Int. J. Energy Res. 45 (2021) 6644–6688. https://doi.org/10.1002/er.6353.

[12] Z.F. Pan, L. An, T.S. Zhao, Z.K. Tang, Advances and challenges in alkaline anion exchange membrane fuel cells, Prog. Energy Combust. Sci. 66 (2018) 141–175. https://doi.org/10.1016/j.pecs.2018.01.001.

[13] D.R. Dekel, Review of cell performance in anion exchange membrane fuel cells, J. Power Sources. 375 (2018) 158–169.

https://doi.org/10.1016/j.jpowsour.2017.07.117.

[14] Z. Wan, Y. Tao, J. Shao, Y. Zhang, H. You, Ammonia as an effective hydrogen carrier and a clean fuel for solid oxide fuel cells, Energy Convers. Manag. 228 (2021) 113729. https://doi.org/10.1016/j.enconman.2020.113729.

[15] W.S. Chai, Y. Bao, P. Jin, G. Tang, L. Zhou, A review on ammonia, ammonia-hydrogen and ammonia-methane fuels, Renew. Sustain. Energy Rev. 147 (2021) 111254. https://doi.org/10.1016/j.rser.2021.111254.

[16] D.R. MacFarlane, P. V. Cherepanov, J. Choi, B.H.R. Suryanto, R.Y. Hodgetts, J.M. Bakker, F.M. Ferrero Vallana, A.N. Simonov, A Roadmap to the Ammonia Economy, Joule. 4 (2020) 1186–1205. https://doi.org/10.1016/j.joule.2020.04.004.

[17] A. Valera-Medina, H. Xiao, M. Owen-Jones, W.I.F. David, P.J. Bowen, Ammonia for power, Prog. Energy Combust. Sci. 69 (2018) 63–102. https://doi.org/10.1016/j.pecs.2018.07.001.

[18] S.S. Rathore, S. Biswas, D. Fini, A.P. Kulkarni, S. Giddey, Direct ammonia solid-oxide fuel cells: A review of progress and prospects, Int. J. Hydrogen Energy. 46 (2021) 35365–35384. https://doi.org/10.1016/j.ijhydene.2021.08.092.

[19] X. Mao, J. Sang, C. Xi, Z. Liu, J. Yang, W. Guan, J. Wang, C. Xia, S.C. Singhal, Performance evaluation of ammonia-fueled flat-tube solid oxide fuel cells with different build-in catalysts, Int. J. Hydrogen Energy. 47 (2022) 23324–23334. https://doi.org/10.1016/j.ijhydene.2022.04.185.

[20] Z. Hu, Q. Xiao, D. Xiao, Z. Wang, F. Gui, Y. Lei, J. Ni, D. Yang, C. Zhang, P. Ming, Synthesis of Anti-poisoning Spinel Mn-Co-C as Cathode Catalysts for Low-Temperature Anion Exchange Membrane Direct Ammonia Fuel Cells, ACS Appl. Mater. Interfaces. 13 (2021) 53945–53954. https://doi.org/10.1021/acsami.1c16251.

[21] R.H. Dolan, J.E. Anderson, T.J. Wallington, Outlook for ammonia as a sustainable transportation fuel, Sustain. Energy Fuels. 5 (2021) 4830–4841. https://doi.org/10.1039/d1se00979f.

[22] E.J. Cairns, E.L. Simons, A.D. Tevebaugh, Ammonia–oxygen fuel cell, Nature. 217 (1968) 780–781.

[23] G. Jeerh, M. Zhang, S. Tao, Recent progress in ammonia fuel cells and their potential applications, J. Mater. Chem. A. 9 (2021) 727–752. https://doi.org/10.1039/d0ta08810b.

[24] Y. Guo, Z. Pan, L. An, Carbon-free sustainable energy technology: Direct ammonia fuel cells, J. Power Sources. 476 (2020) 228454. https://doi.org/10.1016/j.jpowsour.2020.228454.

[25] J.C.M. Silva, S.G. Da Silva, R.F.B. De Souza, G.S. Buzzo, E. V. Spinacé, A.O. Neto, M.H.M.T. Assumpção, PtAu/C electrocatalysts as anodes for direct ammonia fuel cell, Appl. Catal. A Gen. 490 (2015) 133–138. https://doi.org/10.1016/j.apcata.2014.11.015.

[26] Mô.H.M.T. Assumpção, R.M. Piasentin, P. Hammer, R.F.B. De Souza, G.S. Buzzo, M.C. Santos, E. V. Spinacé, A.O. Neto, J.C.M. Silva, Oxidation of

ammonia using PtRh/C electrocatalysts: Fuel cell and electrochemical evaluation, Appl. Catal. B Environ. 174–175 (2015) 136–144. https://doi.org/10.1016/j.apcatb.2015.02.021.

[27] A. Afif, N. Radenahmad, Q. Cheok, S. Shams, J.H. Kim, A.K. Azad, Ammonia-fed fuel cells: A comprehensive review, Renew. Sustain. Energy Rev. 60 (2016) 822–835. https://doi.org/10.1016/j.rser.2016.01.120.

[28] M.H.M.T. Assumpção, S.G. Da Silva, R.F.B. De Souza, G.S. Buzzo, E. V. Spinacé, M.C. Santos, A.O. Neto, J.C.M. Silva, Investigation of PdIr/C electrocatalysts as anode on the performance of direct ammonia fuel cell, J. Power Sources. 268 (2014) 129–136. https://doi.org/10.1016/j.jpowsour.2014.06.025.

[29] R. Lan, S. Tao, Direct ammonia alkaline anion-exchange membrane fuel cells, Electrochem. Solid-State Lett. 13 (2010). https://doi.org/10.1149/1.3428469.

[30] Y. Zhao, B.P. Setzler, J. Wang, J. Nash, T. Wang, B. Xu, Y. Yan, An Efficient Direct Ammonia Fuel Cell for Affordable Carbon-Neutral Transportation, Joule. 3 (2019) 2472–2484. https://doi.org/10.1016/j.joule.2019.07.005.

[31] Y. Li, H.S. Pillai, T. Wang, S. Hwang, Y. Zhao, Z. Qiao, Q. Mu, S. Karakalos, M. Chen, J. Yang, D. Su, H. Xin, Y. Yan, G. Wu, High-performance ammonia oxidation catalysts for anion-exchange membrane direct ammonia fuel cells, Energy Environ. Sci. 14 (2021) 1449–1460. https://doi.org/10.1039/d0ee03351k.

[32] Y. Liu, O.C. Esan, Z. Pan, L. An, Machine learning for advanced energy materials, Energy AI. 3 (2021) 100049.

https://doi.org/10.1016/j.egyai.2021.100049.

[33] A. Legala, J. Zhao, X. Li, Machine learning modeling for proton exchange membrane fuel cell performance, Energy AI. 10 (2022) 100183. https://doi.org/10.1016/j.egyai.2022.100183.

[34] O. Siddiqui, I. Dincer, A review and comparative assessment of direct ammonia fuel cells, Therm. Sci. Eng. Prog. 5 (2018) 568–578. https://doi.org/10.1016/j.tsep.2018.02.011.

[35] R. Lan, S. Tao, Ammonia as a suitable fuel for fuel cells, Front. Energy Res. 2 (2014) 3–6. https://doi.org/10.3389/fenrg.2014.00035.

[36] O.C. Esan, X. Shi, Z. Pan, X. Huo, L. An, T.S. Zhao, Modeling and Simulation of Flow Batteries, Adv. Energy Mater. 10 (2020) 1–42. https://doi.org/10.1002/aenm.202000758.

[37] M.G. Santarelli, M.F. Torchio, P. Cochis, Parameters estimation of a PEM fuel cell polarization curve and analysis of their behavior with temperature, J. Power Sources. 159 (2006) 824–835. https://doi.org/10.1016/j.jpowsour.2005.11.099.

[38] Z. Pan, Y. Bi, L. An, A cost-effective and chemically stable electrode binder for alkaline-acid direct ethylene glycol fuel cells, Appl. Energy. 258 (2020) 114060. https://doi.org/10.1016/j.apenergy.2019.114060.

[39] R. Chen, S. Zheng, Y. Yao, Z. Lin, W. Ouyang, L. Zhuo, Z. Wang, Performance of direct ammonia fuel cell with PtIr/C, PtRu/C, and Pt/C as anode electrocatalysts under mild conditions, Int. J. Hydrogen Energy. 46 (2021) 27749–27757. https://doi.org/10.1016/j.ijhydene.2021.06.001.

[40] A. Kormányos, F.D. Speck, K.J.J. Mayrhofer, S. Cherevko, Influence of Fuels and pH on the Dissolution Stability of Bifunctional PtRu/C Alloy Electrocatalysts, ACS Catal. 10 (2020) 10858–10870. https://doi.org/10.1021/acscatal.0c02094.

[41] F. Isorna Llerena, A. de las Heras Jiménez, E. López González, F. Segura Manzano, J.M. Andújar Márquez, Effects of Ammonia Impurities on the Hydrogen Flow in High and Low Temperature Polymer Electrolyte Fuel Cells, Fuel Cells. 19 (2019) 651–662. https://doi.org/10.1002/fuce.201900031.

[42] T. Wang, Y. Zhao, B.P. Setzler, Y. Yan, Improving Performance and Durability of Low Temperature Direct Ammonia Fuel Cells: Effect of Backpressure and Oxygen Reduction Catalysts, J. Electrochem. Soc. 168 (2021) 014507. https://doi.org/10.1149/1945-7111/abdcca.

[43] L. An, R. Chen, Direct formate fuel cells: A review, J. Power Sources. 320 (2016) 127–139. https://doi.org/10.1016/j.jpowsour.2016.04.082.

[44] C. Song, Y. Tang, J.L. Zhang, J. Zhang, H. Wang, J. Shen, S. McDermid, J. Li, P. Kozak, PEM fuel cell reaction kinetics in the temperature range of 23-120 °C, Electrochim. Acta. 52 (2007) 2552–2561. https://doi.org/10.1016/j.electacta.2006.09.008.

[45] J. Pan, S. Lu, Y. Li, A. Huang, L. Zhuang, J. Lu, High-Performance alkaline polymer electrolyte for fuel cell applications, Adv. Funct. Mater. 20 (2010) 312–319. https://doi.org/10.1002/adfm.200901314.

[46] T.S. Zhao, C. Xu, R. Chen, W.W. Yang, Mass transport phenomena in direct

methanol fuel cells, Prog. Energy Combust. Sci. 35 (2009) 275–292. https://doi.org/10.1016/j.pecs.2009.01.001.

[47] C. Xu, Y.L. He, T.S. Zhao, R. Chen, Q. Ye, Analysis of Mass Transport of Methanol at the Anode of a Direct Methanol Fuel Cell, J. Electrochem. Soc. 153 (2006) A1358. https://doi.org/10.1149/1.2201467.

[48] I. Dincer, O. Siddiqui, Ammonia Fuel Cells, Elsevier, 2020.

[49] R. Abbasi, B.P. Setzler, J. Wang, Y. Zhao, T. Wang, S. Gottesfeld, Y. Yan, Low-temperature direct ammonia fuel cells: Recent developments and remaining challenges, Curr. Opin. Electrochem. 21 (2020) 335–344. https://doi.org/10.1016/j.coelec.2020.03.021.

[50] Y. Shan, S.Y. Choe, A high dynamic PEM fuel cell model with temperature effects, J. Power Sources. 145 (2005) 30–39. https://doi.org/10.1016/j.jpowsour.2004.12.033.

[51] L. Song, Z. Liang, Z. Ma, Y. Zhang, J. Chen, R.R. Adzic, J.X. Wang, Temperature-Dependent Kinetics and Reaction Mechanism of Ammonia Oxidation on Pt, Ir, and PtIr Alloy Catalysts, J. Electrochem. Soc. 165 (2018) J3095–J3100. https://doi.org/10.1149/2.0181815jes.

[52] L. Xu, C. Fang, J. Li, M. Ouyang, W. Lehnert, Nonlinear dynamic mechanism modeling of a polymer electrolyte membrane fuel cell with dead-ended anode considering mass transport and actuator properties, Appl. Energy. 230 (2018) 106–121. https://doi.org/10.1016/j.apenergy.2018.08.099.

[53] O.C. Esan, X. Shi, X. Su, Y. Dai, L. An, T.S. Zhao, A computational model of a

liquid e-fuel cell, J. Power Sources. 501 (2021) 230023. https://doi.org/10.1016/j.jpowsour.2021.230023.

Figures captions:

Fig. 1. (a) Working principles of direct ammonia fuel cells. (b) Schematic of direct ammonia fuel cells.

Fig. 2. Polarization and power density curves.

Fig. 3. Polarization and power density curves at various KOH concentrations.

Fig. 4. Polarization and power density curves at various ammonia concentrations.

Fig. 5. Polarization and power density curves at various oxygen flow rates.

Fig. 6. Polarization and power density curves at various anolyte flow rates.

Fig. 7. Polarization and power density curves at various operating temperatures.

Fig. 8. The constant-current discharging curve at a current density of 20.0 mA cm^{-2}.

Figures

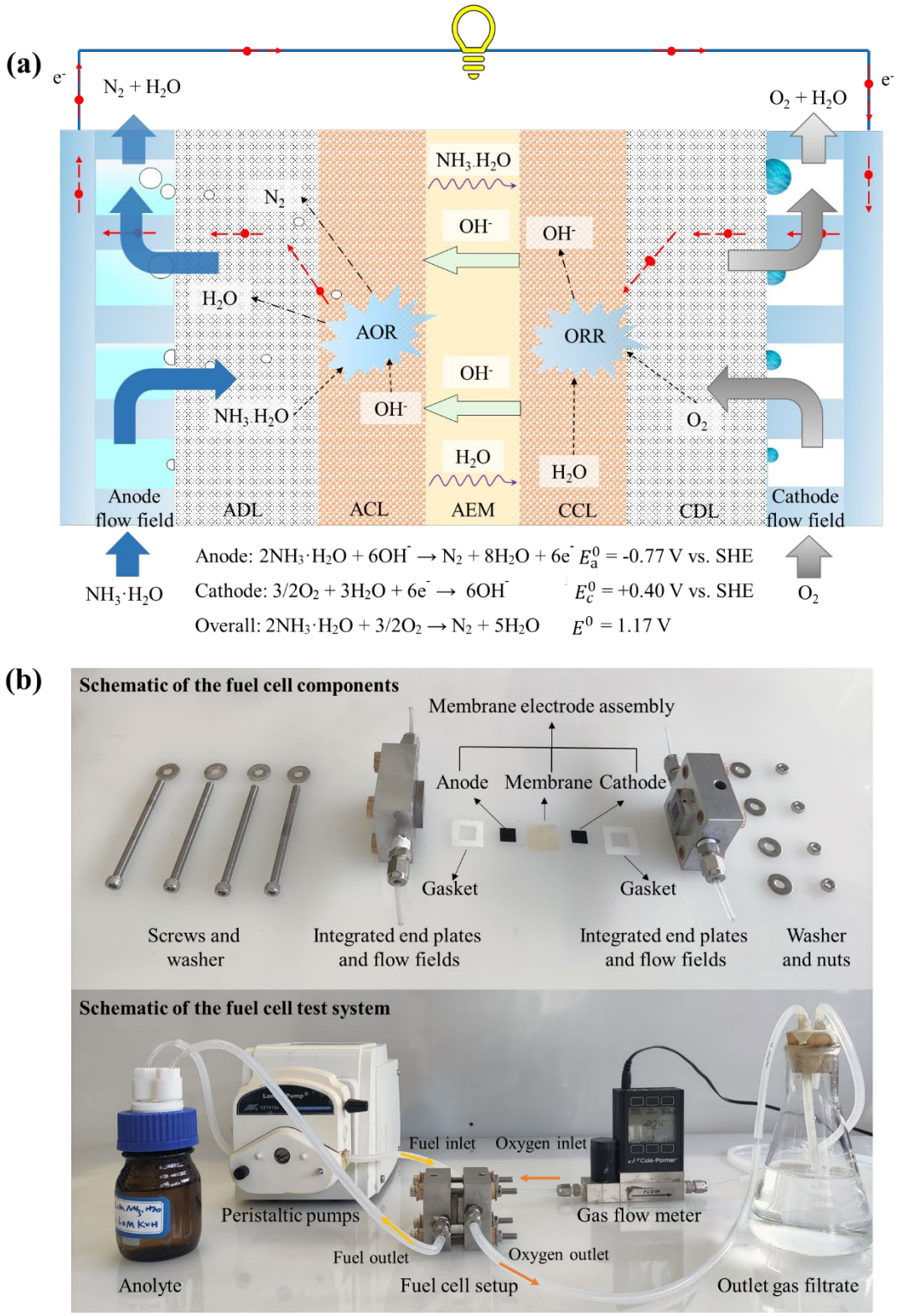

Fig. 1. (a) Working principles of direct ammonia fuel cells. (b) Schematic of direct ammonia fuel cells.

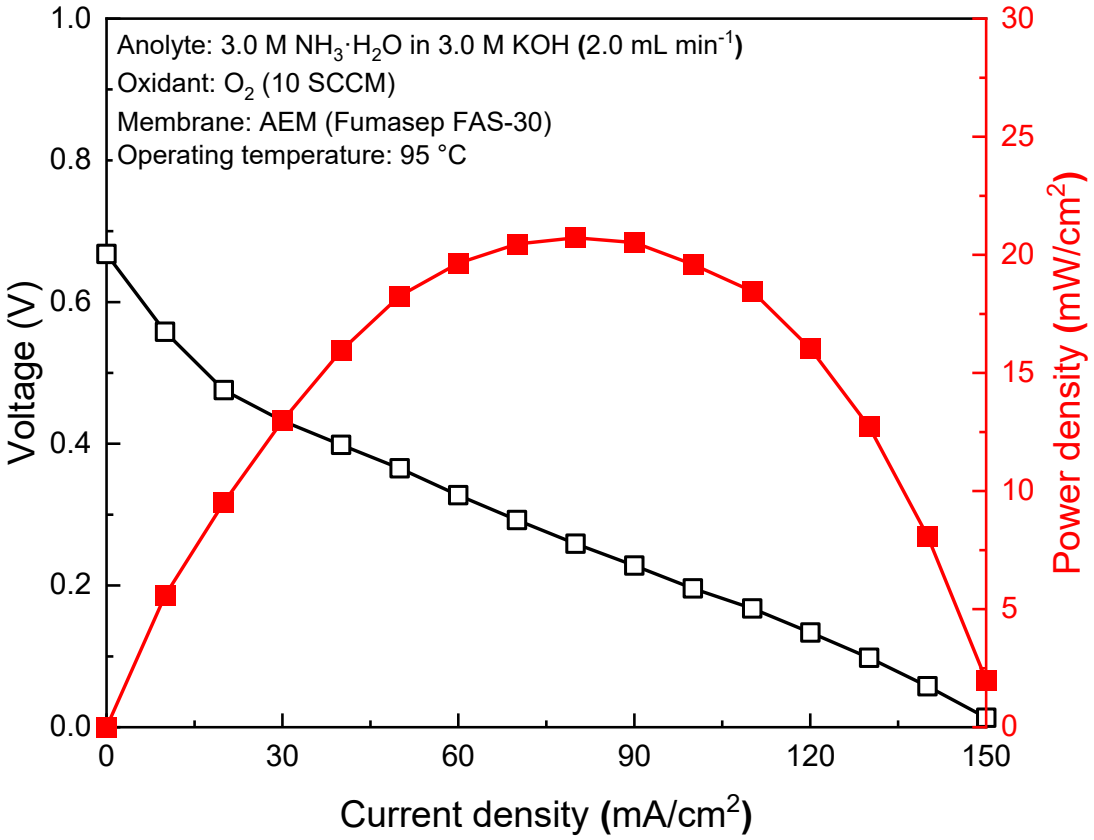

Fig. 2. Polarization and power density curves.

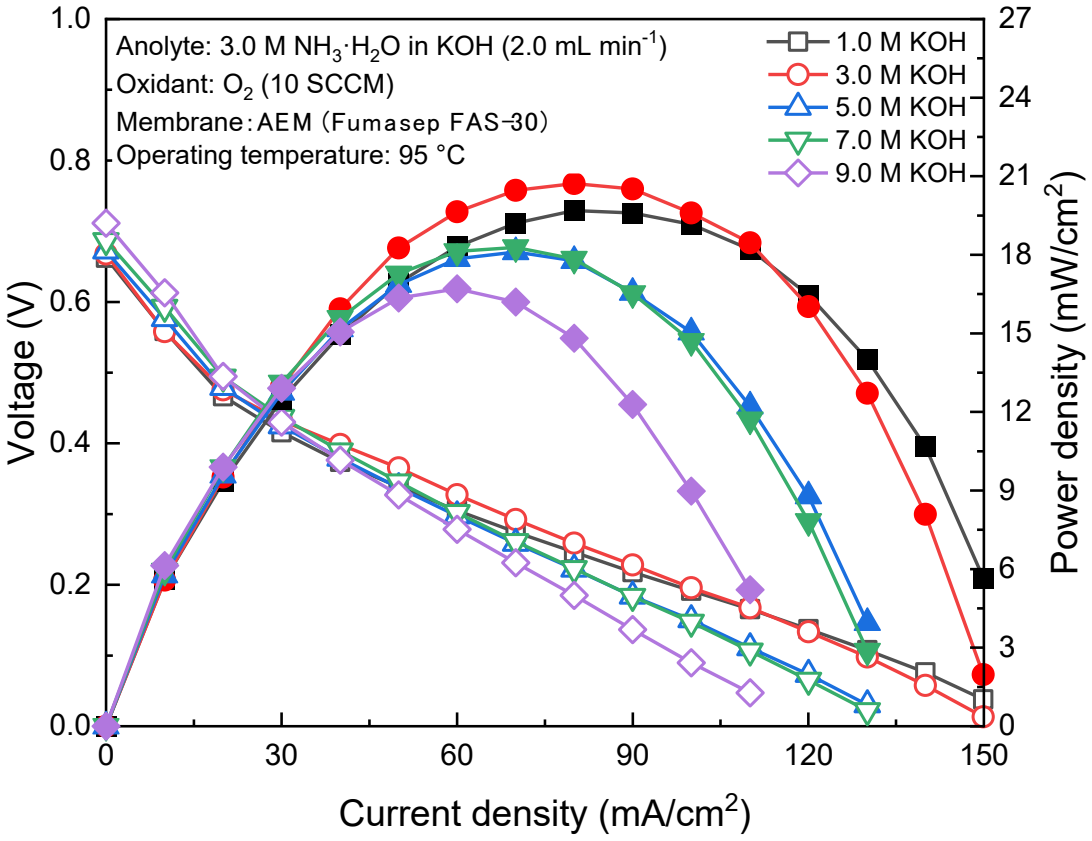

Fig. 3. Polarization and power density curves at various KOH concentrations.

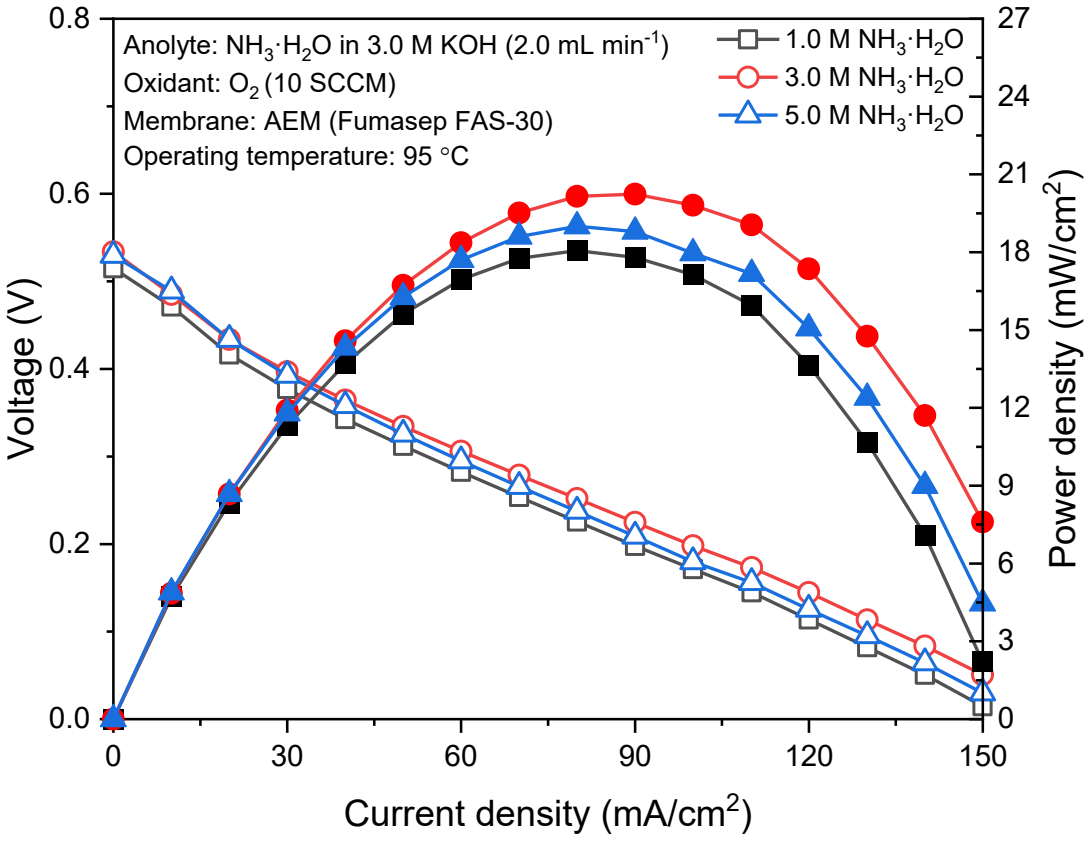

Fig. 4. Polarization and power density curves at various ammonia concentrations.

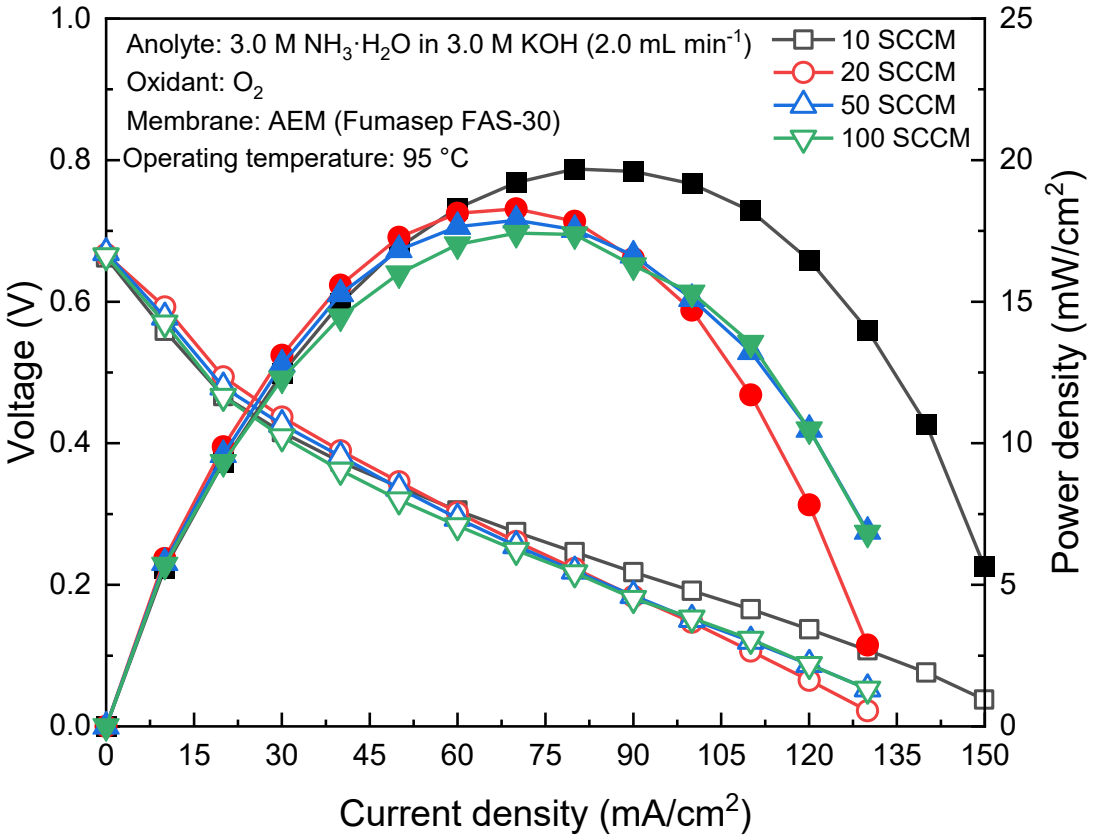

Fig. 5. Polarization and power density curves at various oxygen flow rates.

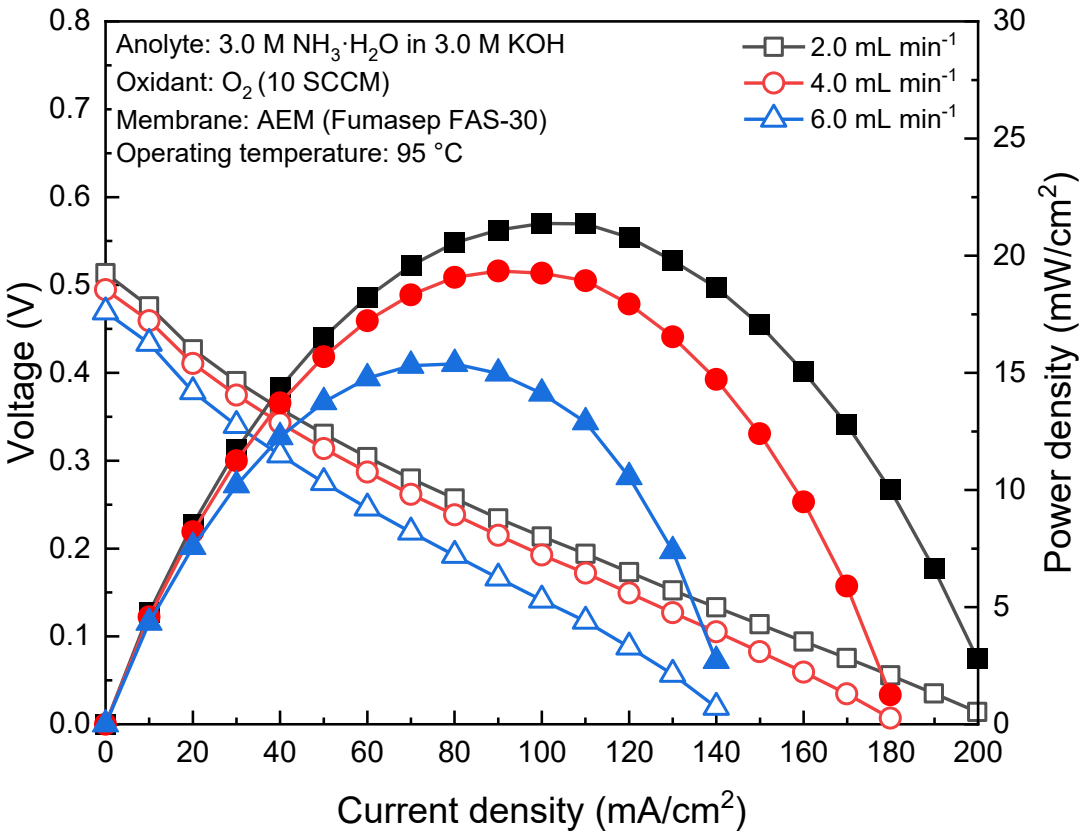

Fig. 6. Polarization and power density curves at various anolyte flow rates.

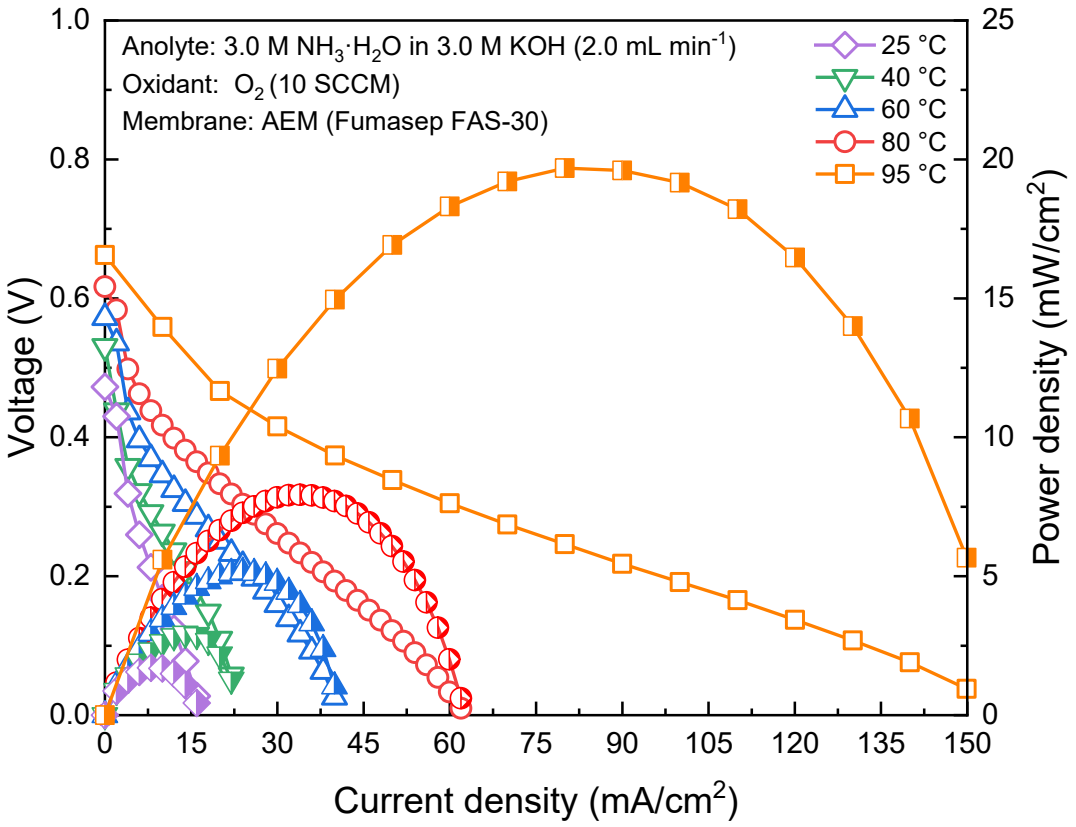

Fig. 7. Polarization and power density curves at various operating temperatures.

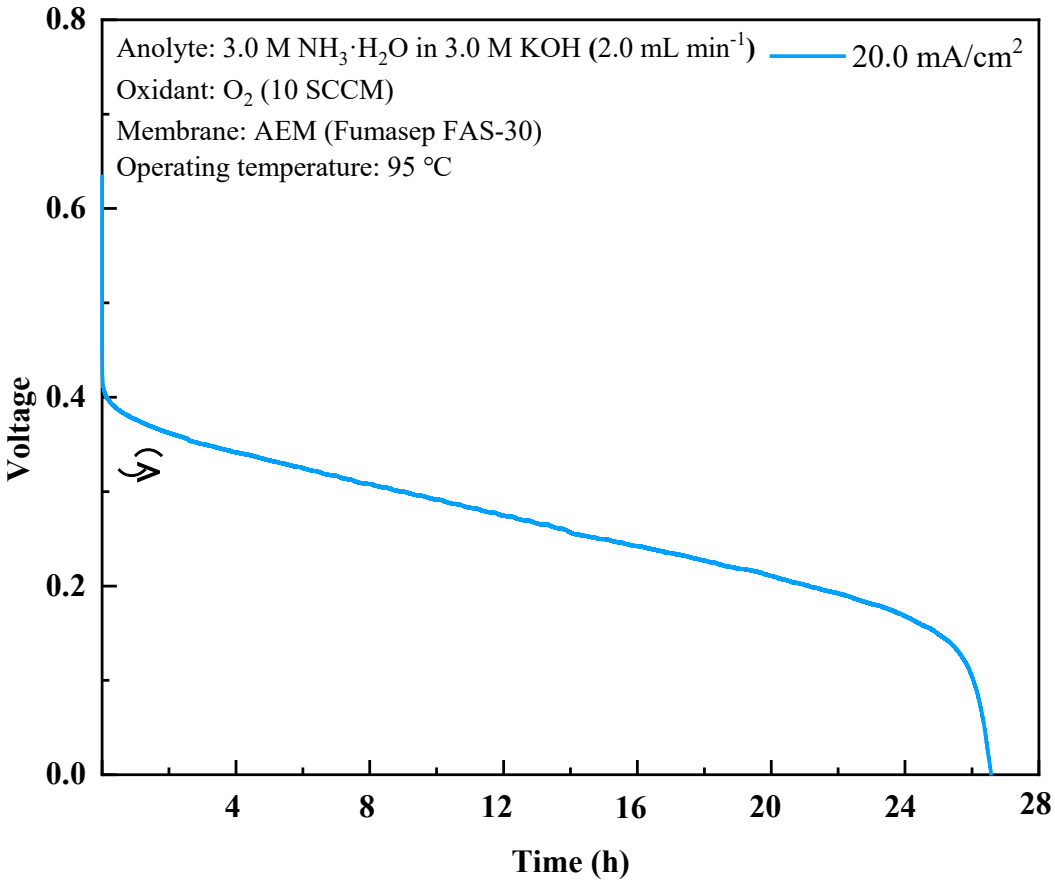

Fig. 8. The constant-current discharging curve at a current density of 20.0 mA cm^{-2}.